Principal Component Analysis to Determine the Surface Properties that Influence the Self-Cleaning Action of Hydrophobic Plant Leaves

Fabien Saubade[a], Lisa I. Pilkington[b], Christopher M. Liauw[a], Luciana C. Gomes[c], Jake McClements[d], Marloes Peeters[d], Mohamed El Mohtadi[e] Filipe Mergulhão[c] and Kathryn A. Whitehead[a]*

[a] Microbiology at Interfaces, Department of Life Sciences, Manchester Metropolitan University, Manchester, UK.

[b] School of Chemical Sciences, University of Auckland, Auckland 1010, New Zealand

[c] LEPABE— Laboratory for Process Engineering, Environment, Biotechnology and Energy, Faculty of Engineering, University of Porto, Rua Dr.Roberto Frias, 4200-465 Porto, Portugal

[d] School of Engineering, Newcastle University, Merz Court, Claremont Road, Newcastle Upon Tyne NE1 7RU, UK

[e] Department of Biology, Edge Hill University, Ormskirk, Lancashire, L39 4QP, UK

*Corresponding Author: K. A. Whitehead, Manchester Metropolitan University, UK.

E-mail address K.A.Whitehead@mmu.ac.uk

ABSTRACT

It is well established that many leaf surfaces display self-cleaning properties. However, an understanding of how the surface properties interact is still confounding. Consequently, twelve different leaf types were selected for analysis due to their water repellency and self-cleaning properties. The most hydrophobic surfaces demonstrated splitting of the v_s CH_2 and v CH_2 bands, ordered platelet-like structures, crystalline waxes, high surface roughness values, high total surface free energy and apolar components of surface energy, and low polar and Lewis base components of surface energy. The surfaces that exhibited the least roughness and high polar and Lewis base components of surface energy had intracuticular waxes, yet still demonstrated self-cleaning action. Principal component analysis demonstrated that the most hydrophobic species shared common surface chemistry traits with low intra-class variability, whilst the less hydrophobic leaves had highly-variable surface chemistry characteristics. Despite this, we have shown through partial least squares regression that leaf water contact angle (i.e. hydrophobicity) can be predicted using attenuated total reflectance Fourier transform infrared spectroscopy surface chemistry data with excellent ability. This is the first time that such a statistical analysis has been performed on a complex biological system. This model could be utilised to investigate and predict the water contact angles of a range of biological surfaces. An understanding of the interplay of properties is extremely important when producing optimised biomimetic surfaces.

Keywords: Biomimetic; plant; roughness; superhydrophobic; wax; self-cleaning.

INTRODUCTION

There has been significant interest directed towards producing biomimetic surfaces with controlled surface wetting properties.[1] Much of this work has concentrated on altering surface topography and chemistry to produce superhydrophobic surfaces. It is generally considered that the topography of plant surfaces is the main factor influencing water contact angle (WCA), and hence water repellency.[2,3] Specifically, hierarchical structures at the macro and micro levels (the Lotus effect) are associated with superhydrophobicity of leaf surfaces.[4] The leaves are also self-cleaning, meaning that rolling droplets can remove microorganisms and other contaminants from their surfaces. Numerous biomimetic surfaces have been developed which emulate the topography of superhydrophobic leaves to achieve self-cleaning, water repellency, and anticontamination properties.[5–8] However, many self-cleaning surfaces produced with biomimetic topographies still require chemical modification to exhibit superhydrophobicity. Many plant surfaces are hydrophobic (WCA >110°) or superhydrophobic (WCA > 150°).[9] However, in nature, there are also several leaf surfaces that display self-cleaning and water-repellent behaviours, and yet they are not superhydrophobic and may not have predominant topographical features.

It is well established that the wax layer on leaf surfaces, in particular epicuticular wax crystals, makes an essential contribution to surface hydrophobicity.[10] The chemical compositions of such waxes from numerous leaf surfaces have been determined.[11–17] However, the exact relationship between surface chemistry and topography, in addition to their influence on surface physiochemistry is not fully understood. Consequently, producing biomimetic surfaces that maintain their anti-wetting features still presents a significant challenge. Thus, an understanding of the key surface properties that result in the water repellency of natural surfaces is essential to further the development of biomimetic surfaces.

The aim of this work was to determine the relationship between the surface topography, chemistry, and physiochemistry of a selection of plant leaves that demonstrated self-cleaning properties. This was implemented through a combination of complementary experimental techniques and modelling methods to identify the key parameters that resulted in the self-cleaning properties of these natural surfaces. This information is vitally important to many aspects of industry where producing low-cost and consistent biomimetic surfaces is a priority.

EXPERIMENTAL

Leaf collection

Plant leaves were selected based on their ability to repel water. Many leaf types were sprayed with water for 1 min and then immediately assessed. Those that exhibited no residual water droplets or spherical spray droplets on their surfaces were deemed the most hydrophobic, and therefore selected. Leaves from the following plants were collected (Westhoughton, Greater Manchester, UK) between the months of September and November 2017: *Aquilegia vulgaris* (Aquilegia), *Citrus sinensis* (Orange), *Gladiolus hybridus* (Gladioli), *Hosta sieboldiama* (Hosta), *Hyacinthus litwinovii* (Hyacinth), *Ilex aquifolium* (Holly), *Lathyrus odoratus* (Sweet pea), *Lupinus polyphyllus* (Lupin), *Nymphaea odorata* (Water lily), *Pelargonium graveolens* (Geranium), *Prunus laurocerasus* (Laurel), and *Rhododendron azaleastrum* (Azalea). Leaf samples were either used within 2-4 h of harvesting or stored at 4 °C for a maximum of 24 h before use. The leaves were stored individually in plastic bags until use to ensure that the loss of humidity from the leaf was reduced. A number of separate batches of mature leaves were collected on different days over the two-month experimental period (n = 10).

Determination of surface energy components

The total surface free energy (γ_s) and the apolar (γ_s^{LW}), polar (γ_s^{AB}), Lewis acid (γ_s^+), and Lewis base (γ_s^-) free energy components of the adaxial surfaces of the leaves were determined using contact angle goniometry. The surface energy components of the leaves were calculated according to the work by van Oss and colleagues.[18-20] A KRÜSS sessile drop goniometer (GH11 KRÜSS, France) was used to perform the measurements with three test liquids: HPLC grade water (BDH, UK), formamide (Sigma-Aldrich, UK), and diiodomethane (Alfa Aesar, UK). For each plant species, except the *Rhododendron azaleastrum*, samples were cut from different parts of the same leaf and attached to microscope slides using double-sided adhesive tape (3M, UK). In the case of *Rhododendron azaleastrum*, individual leaves were used for each test liquid. For all test liquids, the droplet volume was 5 μL and was dispensed using a micro-syringe dedicated to a single solvent.

For each plant species, the van Oss and Good equations were used to obtain the surface energy components from the contact angles of the three test liquids on the leaf surfaces.[18–20] The surface free energy components of these three liquids were taken from Bos et al.[21] (Supporting Information: Table S1).

The contact angles of each test liquid were obtained from five different areas on the leaf, therefore average values were used to obtain the physicochemical parameters. The statistical error in the calculated surface energy components was estimated from the contact angles of each test liquid by using propagation of error principles. The interfacial free energy (ΔG_{iwi}) was used as a measure of the hydrophobicity of a leaf surface where greater (negative) ΔG_{iwi} values related to more hydrophobic surfaces.

Optical profilometry and scanning electron microscopy (SEM)

The surface topographies of the leaves were investigated using a previously described method with a MicroXAM (phase shift) surface mapping microscope (ADE corporation, XYZ

model 4400 ml system, USA).[22] The optical profilometer used an AD phase shift controller (Omniscan, UK). A MAPVIEW AE 2.17 (Omniscan, UK) image analysis system was utilised to obtain the average surface roughness (S_a), root mean square roughness (S_q), and average peak-to-valley roughness (S_{pv}) (n=10).

SEM images were obtained using a Supra 40VP SEM (Carl Zeiss Ltd., UK) with an adapted protocol.[23] The leaf samples were soaked for 24 h at 4 °C in 4 % v/v glutaraldehyde (Agar Scientific, UK). The leaf samples were removed and the excess glutaraldehyde was washed from the leaf surface using sterile water. The leaf samples were then dried overnight. Following drying, the samples were cut into ca. 6 mm^2 coupons. The adaxial sides of the leaves were fixed to carbon pads on SEM stubs (Agar Scientific, UK). The fixed leaf surfaces were sputter coated with gold (Polaron, UK) using the parameters: 5 mA, < 0.1 mbar, and 800 V in argon gas.

Attenuated total reflectance Fourier transform infrared spectroscopy (ATR-FTIR)

ATR-FTIR analysis was performed on leaf samples using a Spectrum Two FT-IR Spectrometer (PerkinElmer, UK) fitted with a UATR single bounce ATR accessory with a diamond (refractive index 2.40) internal reflection element (IRE) (45° angle of incidence) and $LiTaO_3$ detector. For each leaf sample, five different areas were analysed obtaining the spectra over the range of 450 to 4000 cm^{-1}. Spectra were made up of four scans with the resolution set to 4 cm^{-1} and the results were expressed in absorbance. It is worth noting that the penetration depth of the evanescent wave into the leaf surface from the IRE can be estimated to be 1.5 μm at 2900 cm^{-1} and 6.1 μm at 700 cm^{-1}. Calculations based on the equation by F. Mirabella assumed the leaf surface to be mainly hydrocarbon, i.e. paraffin wax (refractive index 1.45).[24] Due to the topographical aspects potentially affecting contact with the IRE, the spectra were not corrected for wavelength dependent penetration depth.

144

145 *Statistical analysis*

146 Error bars were representative of the standard deviation or ± 5% error. One-way
147 analysis of variance (ANOVA) followed by Newman-Keuls tests were performed using R.
148 3.4.1 software. Differences between samples were considered statistically significant for *p*
149 values < 0.05.

150

151 *Principal component analysis (PCA)*

152 PCA was carried out on the ATR-FTIR data measured using R (version 3.2.2, R Core
153 Team, 2015)[25] and R Studio (version 0.99.486, R Studio Team).[26] PCA analysis was performed
154 using the prcomp function as part of the stats package by singular value decomposition of the
155 centred and scaled data matrix.[25] Results of this analysis were visualised using the factoextra
156 package (version 1.0.5) and ggplot2.[27]

157

158 *Partial least squares regression (PLSR)*

159 PLSR was carried out on the ATR-FTIR data using R (version 3.2.2, R Core Team,
160 2015)[25] and R Studio (version 0.99.486, R Studio Team, 2015).[26] PLSR analysis was performed
161 using the plsr function as part of the pls package (version 2.7-1).[28] The kernel algorithm was
162 used on a mean-centred predictor and response data matrix. Leave-one-out cross-validation
163 was utilised to optimise the number of components (8) to be used in the final model.

164

165 **RESULTS AND DISCUSION**

166 *Physicochemical properties of the leaf surfaces*

167 The physicochemical parameter values are represented in radar graphs (Figure 1) to
168 provide a physicochemical map for each leaf surface. Furthermore, the physicochemical

169 parameters of the twelve leaf surfaces are presented in Table 1. The γ_s^{LW} values of all the leaves
170 were higher than their corresponding γ_s^{AB} values. Therefore, all the leaves investigated had
171 non-polar adaxial surfaces. The three most hydrophobic leaves (*Gladiolus hybridus*, *Lupinus*
172 *polyphyllus*, and *Lathyrus odoratus*) demonstrated high γ_s^{LW} values and substantially lower
173 γ_s^{AB}, γ_s^{+}, and γ_s^{-} values. These patterns were represented in the graphs in Figure 1 by thin
174 asymmetric diamond shapes with the long arm pointing upwards. The base and short downward
175 arm of the diamond was formed from the relatively insignificant γ_s^{AB}, γ_s^{+}, and γ_s^{-} contributions
176 to the total surface energy. The less hydrophobic surfaces had higher γ_s^{-} values which led to
177 graphs with wider bases and various triangular shapes.
178

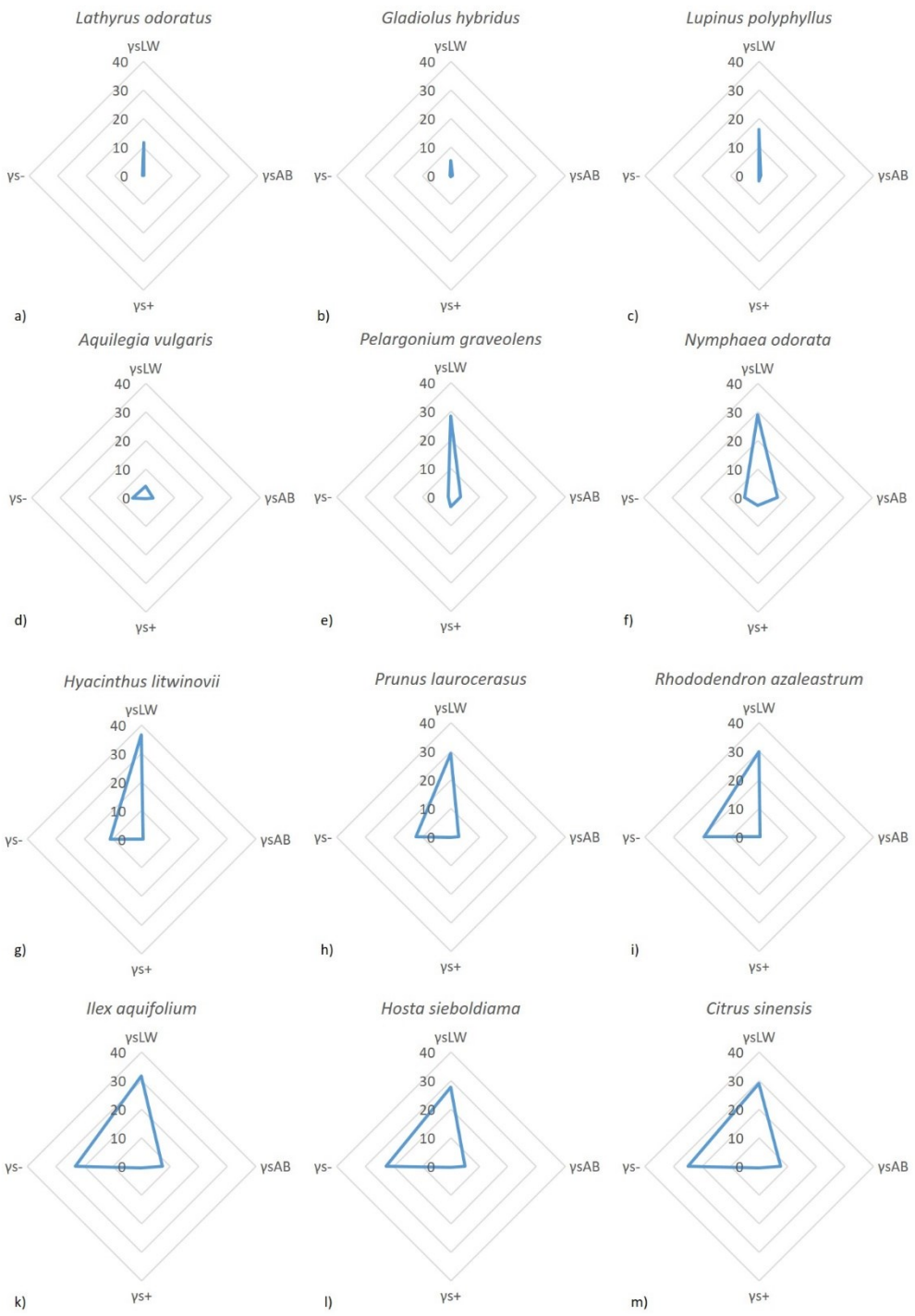

179

180 **Figure 1.** Radar graphs showing the magnitude of the surface energy components for each leaf

181 type.

182

Table 1. Physicochemical parameters of the adaxial surface of the leaf samples. The values are expressed in mJ/m^2 and the errors are in parenthesis.

Leaf	ΔG_{iwi}		γ_s		γ_s^{LW}		γ_s^{AB}		γ_s^+		γ_s^-	
Lathyrus odoratus	-91.7	(9.4)	11.6	(1.0)	11.6	(0.9)	0.1	(0.3)	0.0	(0.0)	0.38	(0.43)
Gladiolus hybridus	-91.3	(12.2)	6.0	(1.2)	5.4	(1.0)	0.6	(0.7)	0.4	(0.4)	0.25	(0.44)
Lupinus polyphyllus	-74.7	(10.6)	16.4	(1.4)	16.2	(0.7)	0.2	(1.2)	1.8	(0.7)	0.00	(0.06)
Aquilegia vulgaris	-64.2	(16.4)	6.9	(2.1)	4.2	(1.0)	2.7	(1.8)	0.4	(0.4)	4.9	(2.90)
Pelargonium graveolens	-54.0	(7.9)	31.5	(1.5)	28.1	(0.9)	3.4	(1.2)	3.3	(0.7)	0.9	(0.57)
Nymphaea odorata	-41.1	(6.5)	35.9	(1.3)	29.0	(0.9)	6.9	(1.0)	2.6	(0.5)	4.5	(1.01)
Hyacinthus litwinovii	-38.3	(7.9)	37.1	(1.4)	36.6	(0.6)	0.5	(1.3)	0.0	(0.0)	10.9	(1.97)
Prunus laurocerasus	-30.1	(6.8)	32.0	(1.2)	29.1	(0.6)	2.8	(1.1)	0.2	(0.1)	12.2	(1.91)
Rhododendron azaleastrum	-14.5	(11.1)	30.3	(2.3)	29.9	(0.6)	0.4	(2.2)	0.0	(0.0)	19.3	(3.76)
Ilex aquifolium	-6.0	(10.5)	38.8	(2.2)	31.5	(0.6)	7.3	(2.1)	0.6	(0.3)	23.1	(3.98)
Hosta sieboldiama	-5.7	(32.6)	32.6	(2.8)	27.6	(1.2)	5.0	(2.6)	0.3	(0.3)	22.8	(3.50)
Citrus sinensis	-2.3	(10.2)	36.4	(2.2)	29.0	(0.6)	7.5	(2.1)	0.6	(0.3)	24.8	(3.99)

Surface topography

The topographies of the leaves were investigated at the macro, micro, and nanoscale scale to comprehensively analyse the morphology of the surface features. Low magnification SEM images (Figure 2) revealed that the macro topographies of the leaves were most commonly characterised by platelet-type features (Figure 2a, g, j, m, p, s, ee, and hh). However, some exhibited quite different surface topographies, including homogenous distributions of raised nodules (Figure 2d), subtle network structures (Figure 2v and y), and very flat, almost featureless surfaces (Figure 2bb). Optical profilometry images highlighted the micro topographies of the leaf surfaces and revealed more detailed information regarding the varied

platelet-like morphology. For example, the average platelet feature length ranged from 10 to 45 μm and some were very regular in shape (Figure 2h, n, and ff), whilst others were far more irregular (Figure 2b, k, t, and ii). The nano features of the surface topographies were investigated using high magnification SEM. The images demonstrated that wax nanocrystals were present on all the leaf surfaces in varying amounts. The most hydrophobic surfaces (Figure 2c, 2f, 2i, and 2l) exhibited dense distributions of wax nanocrystals, whilst the less hydrophobic surfaces had far smaller amounts (Figure 2x, aa, dd, gg, and jj).

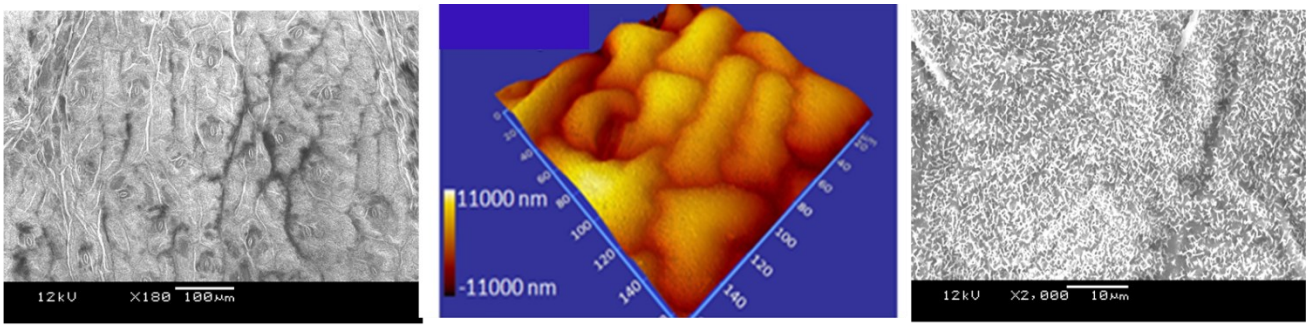

a) *Lathyrus odoratus* b) c)

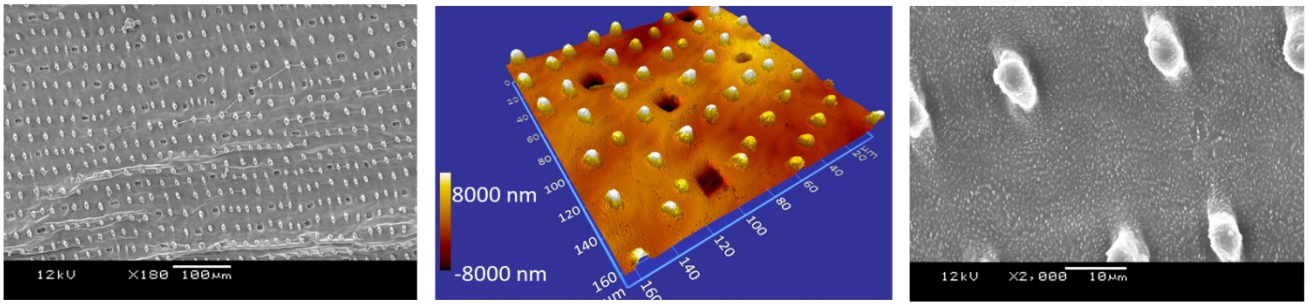

d) *Gladiolus hybridus* e) f)

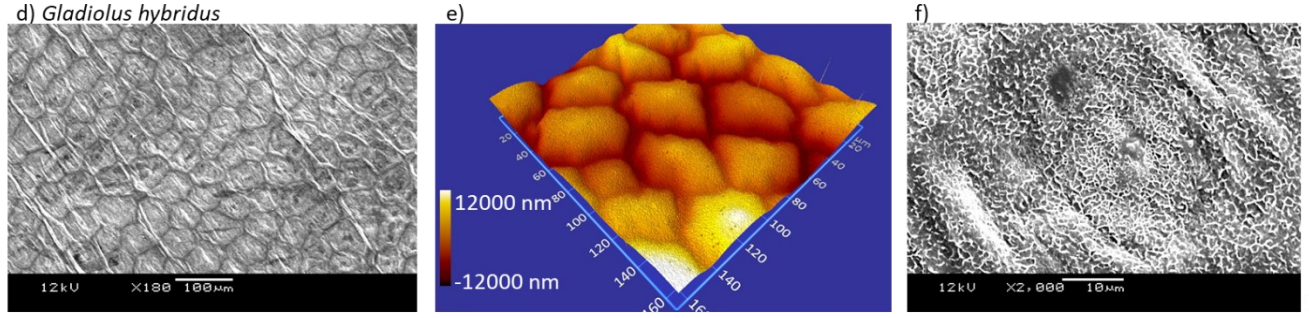

g) *Lupinus polyphyllus* h) i)

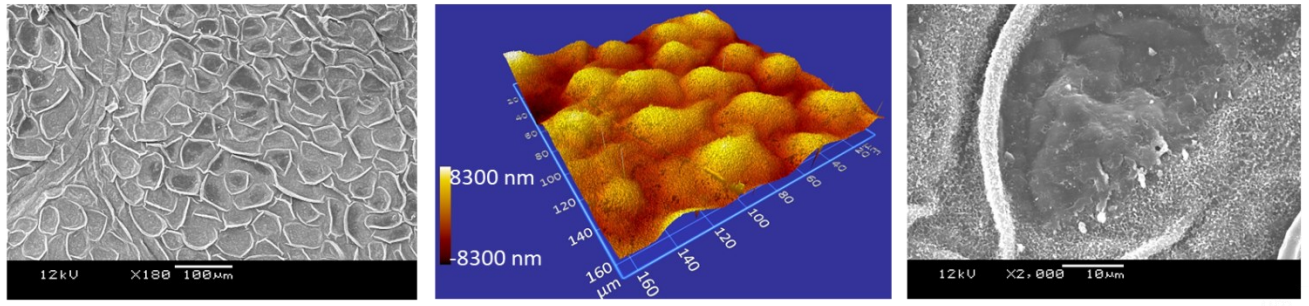

j) *Aquilegia vulgaris* k) l)

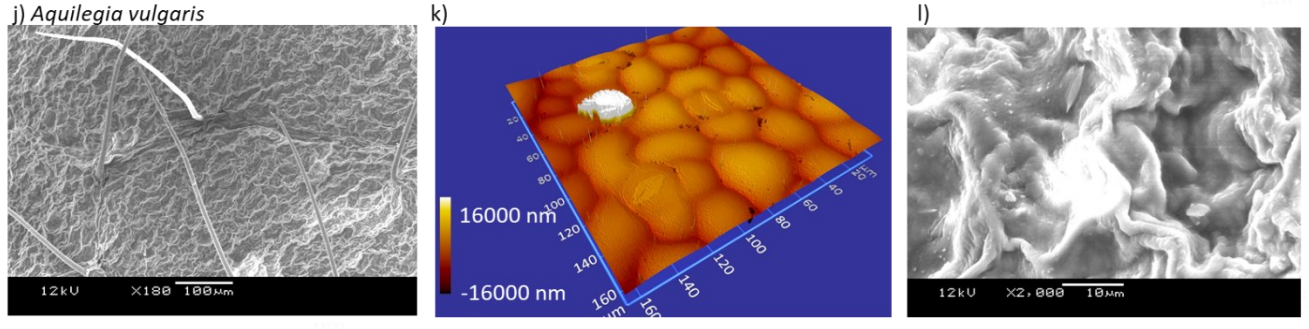

m) *Pelargonium graveolens* n) o)

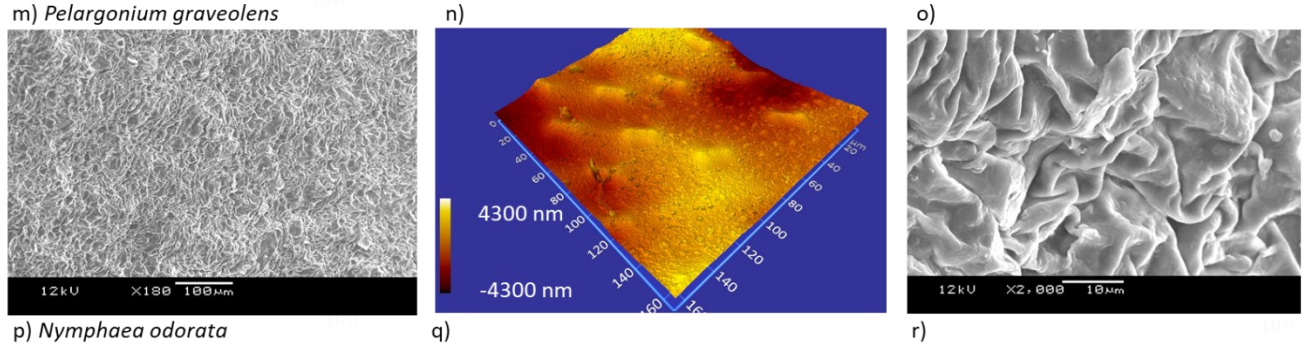

p) *Nymphaea odorata* q) r)

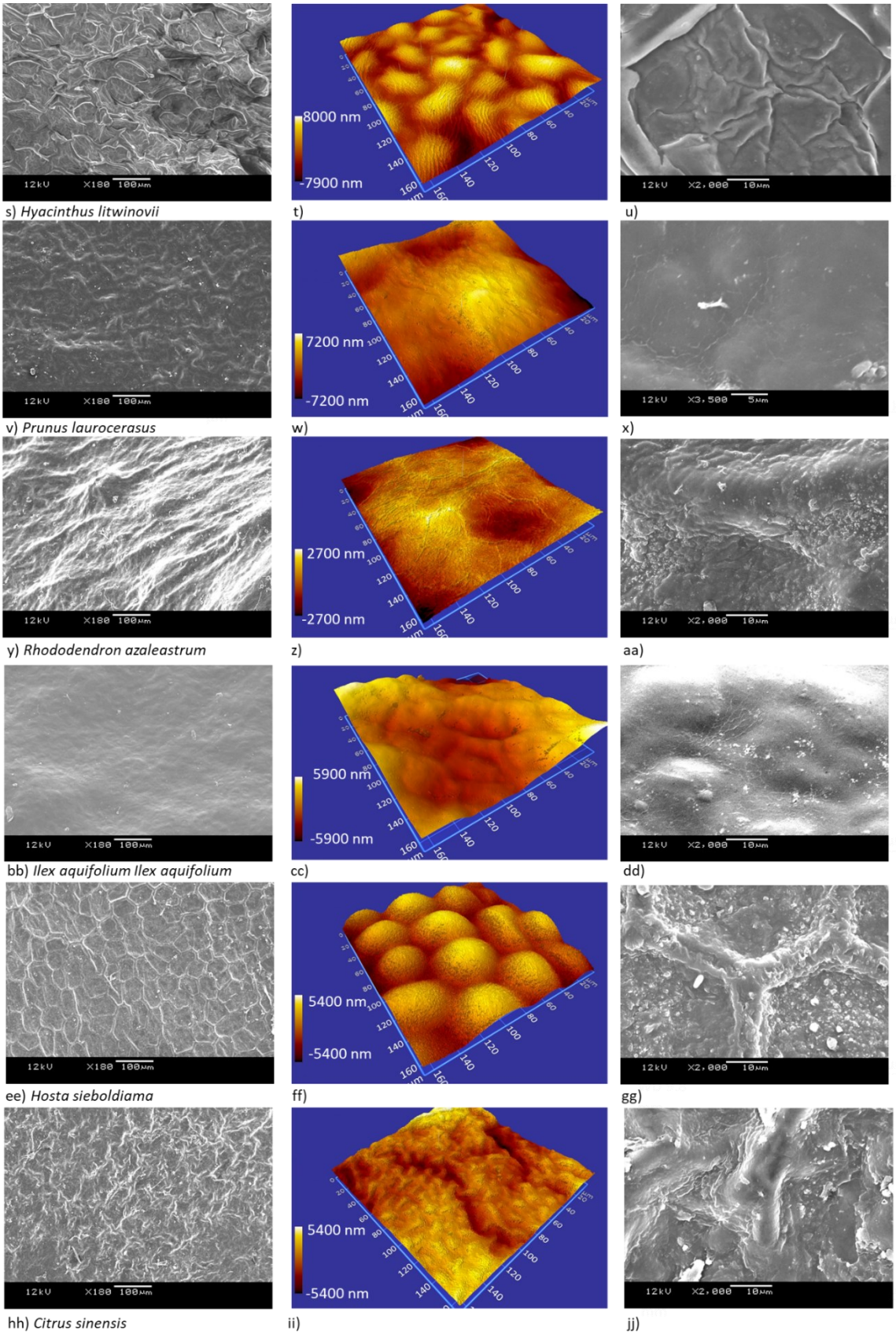

Figure 2. Optical profilometry and SEM images of the adaxial surfaces of the leaf samples demonstrating their macro, micro, and nano surface topographies.

207 Table 3 presents the surface roughness values for each leaf type. The results demonstrate that
208 the more hydrophobic surfaces generally had the greatest roughness values, whilst the least
209 hydrophobic surfaces had the lowest roughness values. However, there were some exceptions
210 to this trend. For example, the *Pelargonium graveolens* had the largest roughness values.
211 Similarly, the *Hyacinthus litwinovii* leaf, which was not one of the most hydrophobic surfaces,
212 also had large S_a (2.8 μm) and S_{pv} (118.9 μm) values. Generally, the least hydrophobic surfaces
213 had less defined surface features. The exception was the *Hosta sieboldiama*, which had low
214 surface roughness values but still demonstrated defined platelet-type features on its surface
215 (Figure 2n).
216
217 **Table 3.** Surface roughness parameters of the leaf samples obtained from the optical
218 profilometry data. The standard deviations are indicated in parenthesis.

Leaf	S_a (μm)	S_q (μm)	S_{pv} (μm)
Lathyrus odoratus	3.2 (0.6)	3.9 (0.7)	36.5 (8.5)
Gladiolus hybridus	2.6 (0.9)	3.6 (1.1)	69.2 (20.1)
Lupinus polyphyllus	4.3 (1.4)	5.3 (1.8)	41.1 (10.1)
Aquilegia vulgaris	2.9 (0.4)	3.6 (0.6)	41.5 (8.1)
Pelargonium graveolens	5.9 (1.5)	9.4 (2.0)	148.2 (15.2)
Nymphaea odorata	0.8 (0.1)	1.1 (0.2)	9.9 (3.0)
Hyacinthus litwinovii	2.8 (0.9)	3.5 (1.2)	118.9 (19.2)
Prunus laurocerasus	2.0 (0.4)	2.4 (0.4)	13.4 (2.8)
Rhododendron azaleastrum	2.2 (1.1)	2.9 (1.5)	40.0 (21.4)
Ilex aquifolium	1.2 (0.2)	1.4 (0.2)	9.0 (2.0)
Hosta sieboldiama	2.0 (0.4)	2.5 (0.5)	28.8 (11.5)
Citrus sinensis	1.6 (0.4)	2.1 (0.5)	31.9 (18.6)

Surface chemistry

ATR-FTIR was used to identify the major classes of chemical species within the first few microns of the adaxial surfaces of the leaves (Figures 3 and 4). All the leaf spectra generally featured a relatively strong and broad hydrogen-bonded OH stretching band centred at 3300 cm^{-1} (Peak A, Figure 3). For the *Prunus laurocerasus* and *Hosta sieboldiama*, this band was noticeably weak relative to the C-H stretching bands (centred at ca. 2900 cm^{-1}). However, for the *Nymphaea odorata*, the OH band was more intense than the C-H band. The *Gladiolus hybridus*, *Citrus sinensis*, *Hyacinthus litwinovii*, and *Pelargonium graveolens* leaves had an OH band that was of near equal intensity to the C-H band. The OH band can be assigned to alcohols, carboxylic acids, and water. All the leaves exhibited two bands at 2916 and 2846 cm^{-1} (asymmetric (ν_{as} CH_2) and symmetric (ν_s CH_2) methylene C-H stretching, respectively), which corresponded to the non-polar hydrocarbon compounds on their surfaces. The accompanying methylene C-H deformation (scissoring (ν_s CH_2)) and C-H rocking (ρ CH_2) bands centred at ca. 1450 and 720 cm^{-1}, respectively, were also evident. All the leaves featured carbonyl (C=O) bearing species that generally absorbed at 1735 cm^{-1}, indicating the possible dominance of ester-based compounds present in the leaf composition. A broad collection of bands centred at ca. 1630 cm^{-1} was also evident on all the leaves which can be assigned mainly to H-O bending modes of the water molecule. In all cases, except *Hosta sieboldiama* and to a lesser extent *Prunus laurocerasus*, the absorbance of this band was indicative of the OH stretching band. In the exceptional cases of *Hosta sieboldiama* and *Prunus laurocerasus*, there was significant confounding with other chemical species that absorbed in the same region. For *Hosta sieboldiama*, there was a strong and sharp band (1640 cm^{-1}) in this region. For all the leaf surfaces, a band at 1055 cm^{-1} was detected which could correspond to the C–O stretching of primary alcohols that are present.

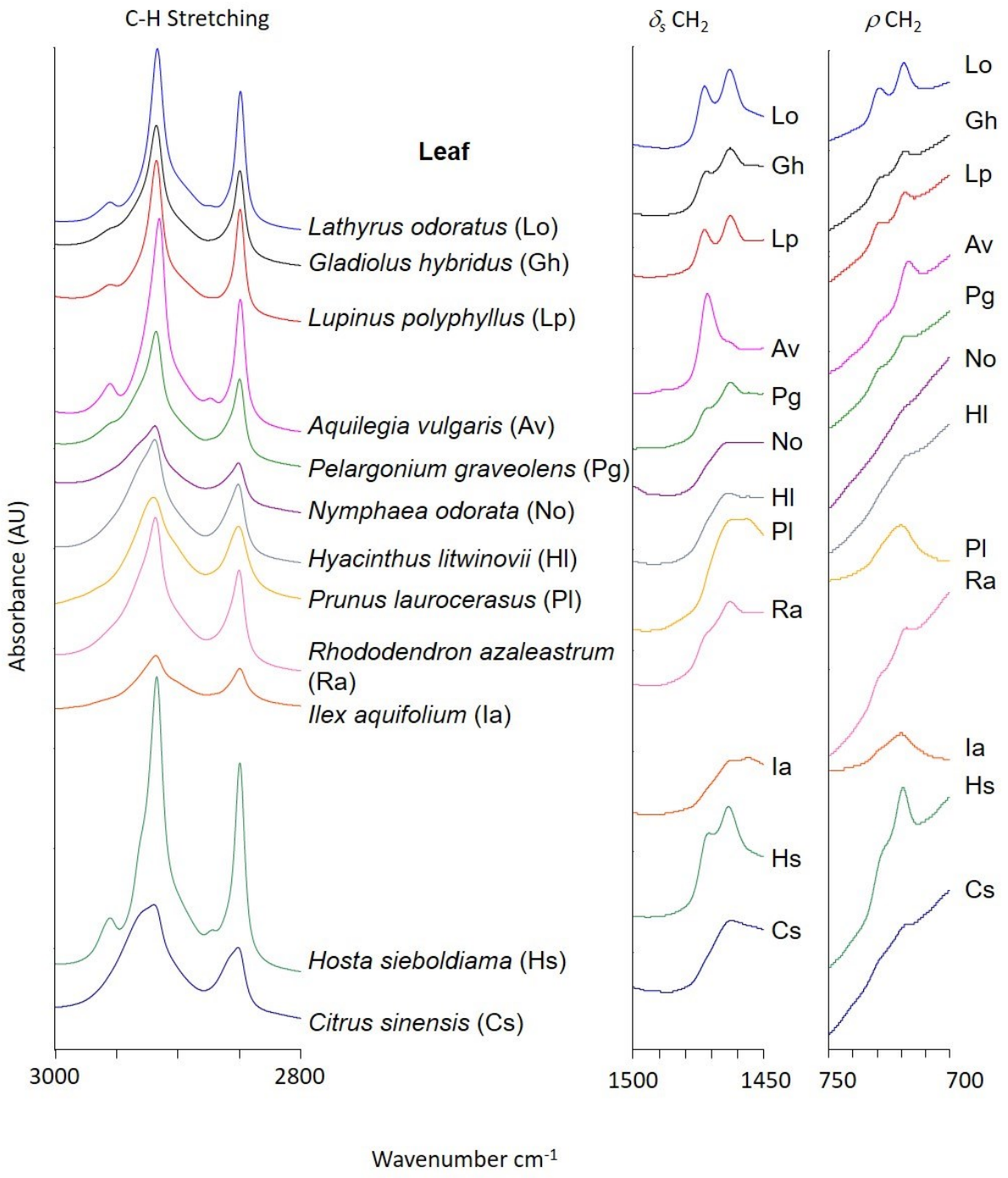

243

244 **Figure 3.** C-H stretching, C-H deformation, and C-H rocking regions of the ATR-FTIR spectra
245 of the leaf samples showing variations in hydrocarbon content and structural ordering of wax
246 components (splitting of the ν_s CH$_2$ and ρ CH$_2$ bands). Lo: *Lathyrus odoratus*, Gh: *Gladiolus*
247 *hybridus*, Lp: *Lupinus polyphyllus*, Av: *Aquilegia vulgaris*, Pg: *Pelargonium graveolens,* No:
248 *Nymphaea odorata*, Hl: *Hyacinthus litwinovii*, Pl: *Prunus laurocerasus*, Ra: *Rhododendron*
249 *azaleastrum*, Ia: *Ilex aquifolium*, Hs: *Hosta sieboldiama,* Cs: *Citrus sinensis*.

A band at 1032 cm^{-1} was detected on the *Lathyrus odoratus*, *Nymphaea odorata*, *Hyacinthus litwinovii*, *Prunus laurocerasus*, *Ilex aquifolium*, *Hosta sieboldiama*, and *Citrus sinensis* leaf surfaces, which could correspond to the C–O stretching of secondary alcohols. Interestingly, pronounced splitting of the ν_s CH_2 and ρ CH_2 bands was detected in the spectra of the *Gladiolus hybridus*, *Hosta sieboldiama*, *Lupinus polyphyllus*, and *Lathyrus odoratus*, which can be assigned to the presence of highly crystalline wax structures (Figure 4). This was also evident on the *Aquilegia vulgaris* and *Pelargonium graveolens* leaf surfaces but to a lesser extent. The *Ilex aquifolium* and *Prunus laurocerasus* surfaces exhibited a single ρ CH_2 band at 719 cm^{-1}, which could indicate a disordered (liquid-like) arrangement of long alkyl chains. The *Hyacinthus litwinovii* and *Nymphaea odorata* showed weak ν_s CH_2 and ρ CH_2 bands hindering detection of splitting. The *Hosta sieboldiama* differed from the other surfaces in that it also demonstrated a ν_{as} CH_2 band at 2925 cm^{-1} and a C=O peak at 1640 cm^{-1}. Overall with regards to the surface chemistries, the molecules observed on all the surfaces were those likely to be related to the cutin structure of the surface.[14] The results demonstrate that the main differences in the surface chemistry were related to the disordered arrangement of wax-like chains (*Prunus laurocerasus* and *Hosta sieboldiama*), in addition to the C=O and ν_{as} CH_2 group of the *Hosta sieboldiama*.

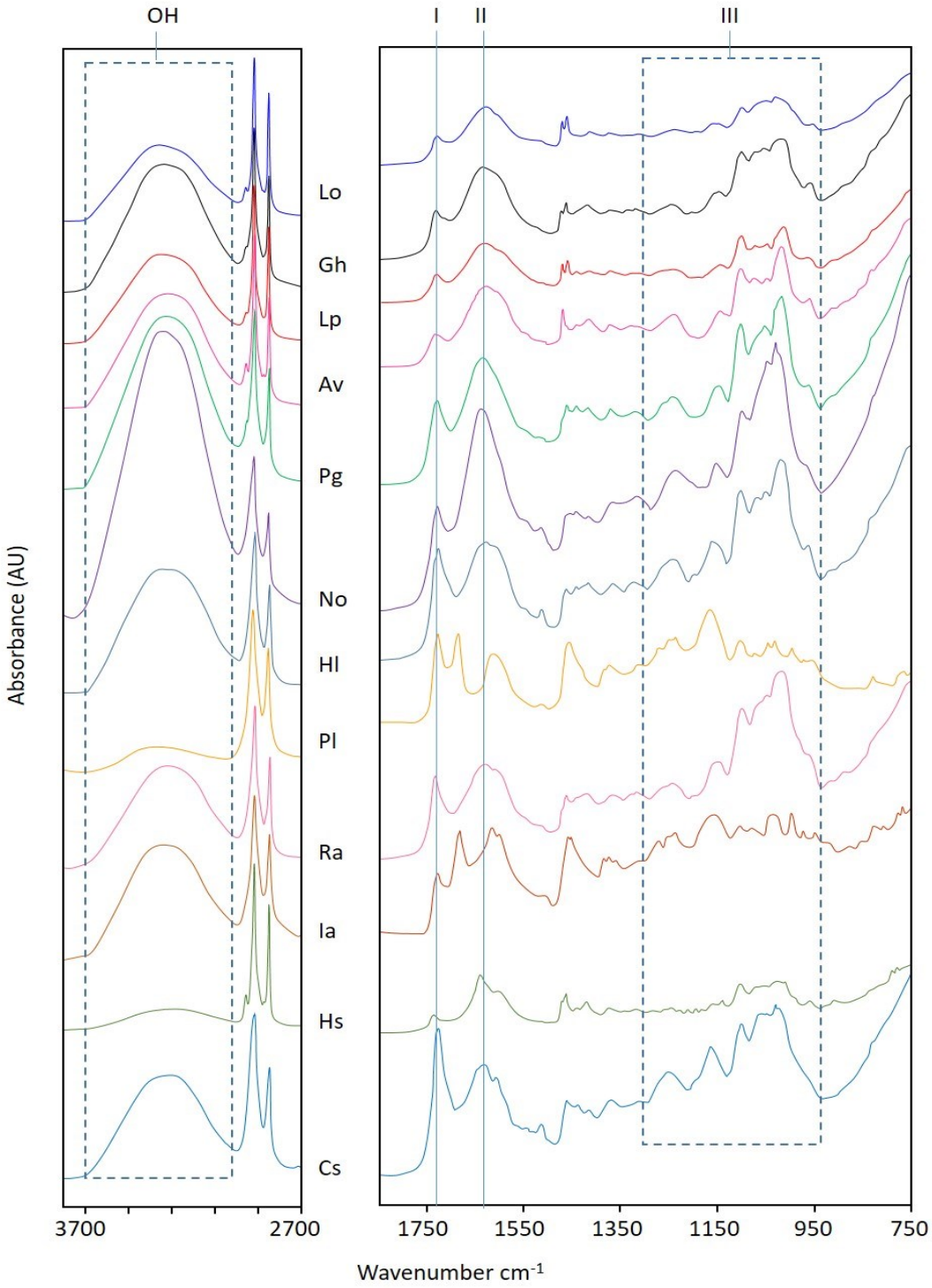

Figure 4. ATR-FTIR spectra showing OH and CH stretching and fingerprint regions of the leaf surfaces (leaf coding is as for Figure 3). Note that absorbance has been normalised to the C-H stretching bands to compensate for differences in effective contact area. Band I: carbonyl stretching from esters and other carbonyl compounds; Band II: assigned to the H-OH bending vibration of water; Bands III: various C-O stretching and C-N stretching vibrations.

Overall, there were some clear demarcations in the surface properties and composition of the leaf samples. The *Lathyrus odoratus*, *Gladiolus hybridus,* and *Lupinus polyphyllus* were the most hydrophobic with ΔG_{iwi} values of -91.7, -91.3, and -74.7 mJ/m^2, respectively. Their surface properties fitted with the Cassie-Baxter model of self-cleaning surfaces and they shared common traits such as high S_a, S_q, and S_{pv} values, and low γ_s^{LW}, γ_s^{AB}, and γ_s^- components. However, the surface topography of the *Lathyrus odoratus* and *Lupinus polyphyllus* was characterised by platelet-like features, whereas the *Gladiolus hybridus* surface was populated by a homogenous distribution of raised nodules. The presence of wax nanocrystals was also evident on all three surfaces. Furthermore, their ATR-FTIR spectra exhibited splitting of the ν_s CH_2 and ν CH_2 bands. This indicated hydrocarbon wax crystallisation, which was in agreement with the SEM images that showed distinct wax crystallisation on their surfaces. Thus, it appeared that a high degree of surface roughness and the presence of a dense population of wax nanocrystals corresponded to a very hydrophobic leaf surface. However, it did not appear that the shape of the surface features distinctly influenced its hydrophobicity. This fits with the Cassie-Baxter model, whereby air (or gas) pockets may be trapped in the cavities of a rough surface, resulting in a hydrophobic surface due to a composite interface with air pockets trapped under the droplet.[30] It has also been suggested that nanoroughness is required to support nanodroplets.[31,32] Thus, it might be likely that an interplay of all these factors resulted in the most hydrophobic surfaces, although the exact parameters that impact this effect are still unclear.

The *Aquilegia vulgaris* was the fourth most hydrophobic surface and had greater γ_s^{AB} and γ_s^- components, as well as less splitting of the ν_s CH_2 and ν CH_2 bands compared with the three most hydrophobic leaves. The *Pelargonium graveolens* was the fifth most hydrophobic surface and the only one with distinct trichomes. The *Pelargonium graveolens* had higher γ_s^{LW}, γ_s^{AB}, and γ_s^+ components than the four most hydrophobic surfaces which is likely influenced by

298 the trichomes on its surface. Godeau et al.[33] observed that the trichomes on *Echeveria pulvinata*
299 leaves were hydrophobic, whilst the surface from which the trichomes protruded was
300 hydrophilic. Water droplets may also rest on the trichomes as perfect spheres which means they
301 can easily run off the leaves.[1]

302 The surfaces with intermediate hydrophobicity (*Nymphaea odorata*, *Hyacinthus*
303 *litwinovii*, *Prunus laurocerasus*, and *Rhododendron azaleastrum*) had mostly featureless
304 topographies, with the exception of the *Hyacinthus litwinovii* (platelet-like features).
305 Furthermore, there were no clear trends in their surface roughness or physicochemical values.
306 From the analysis, it was expected that the *Nymphaea odorata* would have been more
307 hydrophobic. However, the *Nymphaea odorata* surfaces used in this work had very few
308 topographical features. Additionally, compared to the other leaves, the *Nymphaea odorata*
309 surface exhibited intense OH stretching bands in the ATR-FTIR results, which would render
310 the surface more polar, and hence less hydrophobic. This effect may have been due to the age
311 of the leaf,[2,34], thus suggesting that further studies are required to determine the surfaces of
312 leaves over time with respect to changes in their self-cleaning and water repellent properties.
313

314 *PCA and PLSR modelling of surface chemistry data*

315 The ATR-FTIR spectral data provided a basis for further statistical analysis of the
316 leaves. PCA was performed to analyse the results of the ATR-FTIR measurements to provide
317 a greater understanding of the relationships between the variables within the data**.**[29] The PCA
318 data is presented using score plots labelled by leaf type on the top and class (i.e. level of
319 hydrophobicity) on the bottom (Figure 5), in addition to the loading plots of the first three
320 principal components (Figure 6). Analysing the loading plots (Figure 6) for each of the
321 principal components enabled the determination of which section(s)/peaks of the ATR-FTIR
322 spectra were influential in the relative positioning of the leaves in PCA and could be used to

relate back to the original spectra. Additionally, analysing the PCA when categorising the samples according to their classification (surface wettability) revealed that the most hydrophobic leaves shared common surface chemistry traits, demonstrated by being grouped in close proximity with low intra-class variability (Figure 5, bottom). Based on their placement in principal component 1 (PC1), it was concluded that the most hydrophobic leaves had strong peaks pertaining to the OH stretching band, which could be observed when analysing the raw data (Figure 5, bottom). The hydrophobic leaves also exhibited strong asymmetric (ν_{as} CH_2) and symmetric (ν_s CH_2) methylene C-H stretching peaks at ~2916 and ~2846 cm^{-1}, respectively, in addition to weak carbonyl ester peaks at ~1735 cm^{-1}. Furthermore, one of the peaks that was a unique contributor to principal component 3 (PC3) included the split CH_2 peak (~1475 cm^{-1}) methylene asymmetric (ν_{as} CH_2) C-H deformation which was only present in the most hydrophobic leaves. This peak is indicative of non-cutin wax structures. In contrast, the least hydrophobic leaves have highly-variable surface chemistry as measured by ATR-FTIR, demonstrated by their scattered positions in the score plots. Interestingly, with the exception of a few of the leaf samples, the hydrophobic and less-hydrophobic classified leaves could almost be completely separated on the basis of their position according to PC3. This indicated that the characteristics that contributed to this principal component could be used to distinguish between these classifications and that their profile/values for these bands and corresponding functional groups were very important in determining the hydrophobicity of a surface.

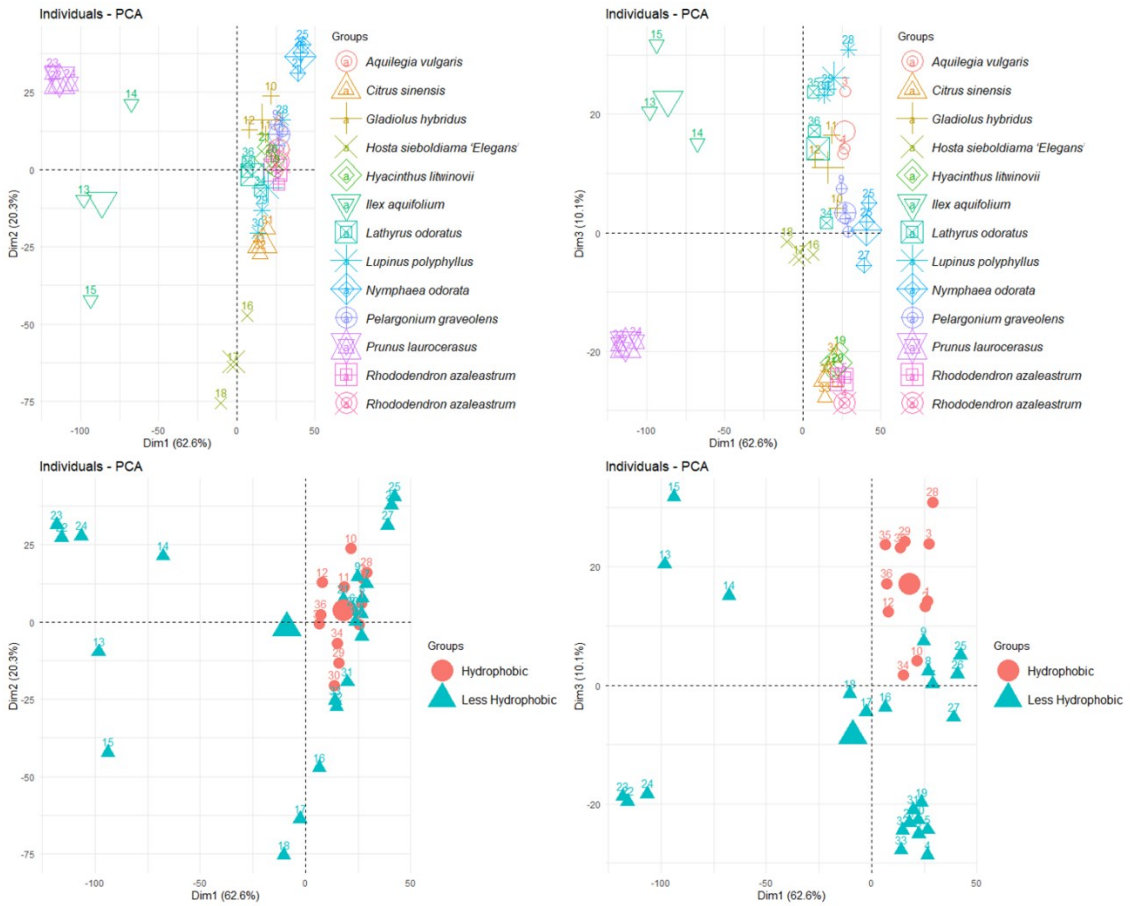

342

343 **Figure 5.** Score plots labelled by leaf type (top) and class, i.e. hydrophobicity, (bottom) of PC1

344 vs PC2 (left) and PC1 vs PC3 (right) for the PCA of the ATR-FTIR spectra.

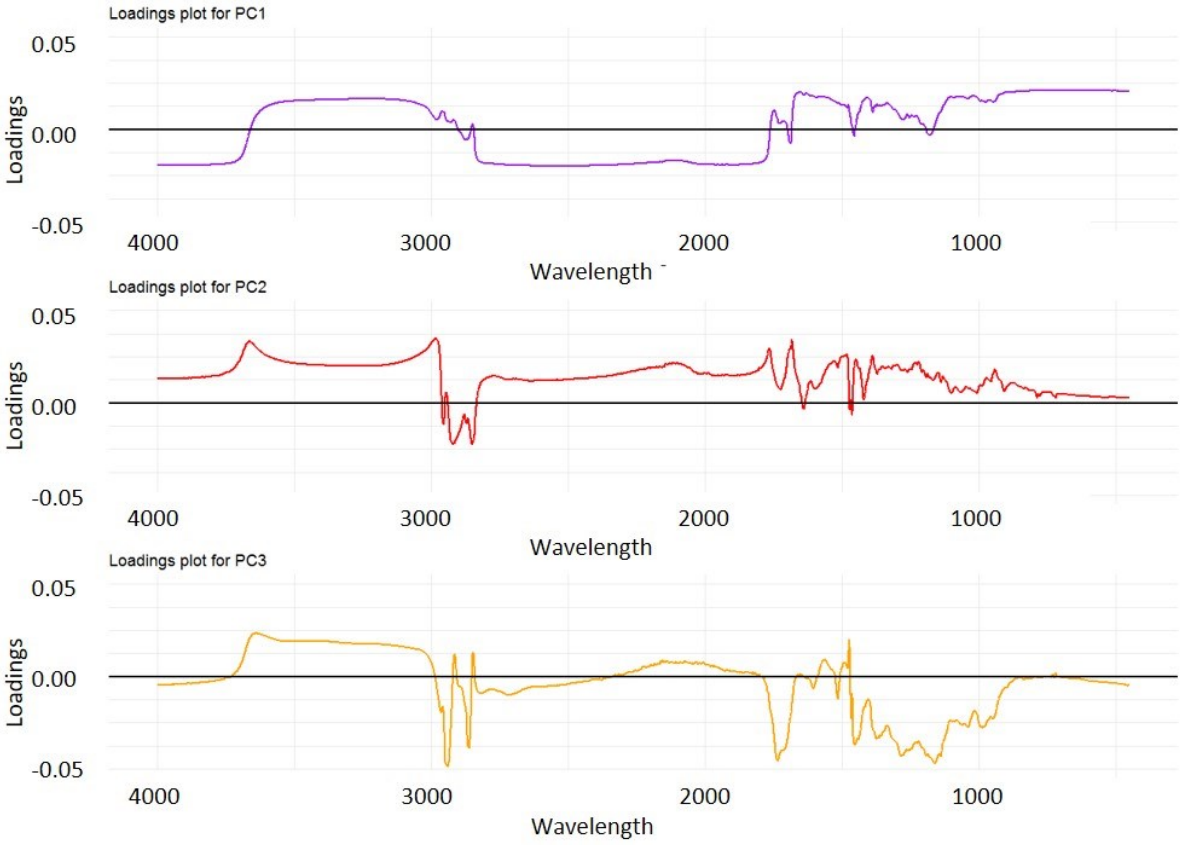

345

346 **Figure 6.** Loading plots for the PCA of the ATR-FTIR spectra of the first three PCs. PC1 (top),
347 PC2 (middle), and PC3 (bottom).

348

349 Assessing the data by leaf type, it was clear that the ATR-FTIR of *Prunus laurocerasus*
350 and *Ilex aquifolium* were very distinct from each other, as well as the other leaves in terms of
351 the components that contribute to PC1 (Figure 5, top). Additionally, the *Hosta sieboldiama*
352 was different from the other leaves (ν_{as} CH_2, C=O) that contributed to PC2. On the
353 determination of which areas of the ATR-FTIR spectra had distinct loadings for PC2 compared
354 to the other PCs, it was observed that PC2 featured (among others) peaks at 2925 and 1640 cm^{-1}
355 (downwards), and was the only PC that had notable influence by peaks in the 800-650 cm^{-1}
356 range (Figure 6 middle). In contrast to the other leaf samples, *Hosta sieboldiama* exhibited a
357 notable peak centred at ~2925 cm^{-1} shouldering the ν_s CH_2 band (ca. 2916 cm^{-1}) and was the
358 only leaf to exhibit a sharp absorption at 1640 cm^{-1}. Furthermore, the *Hosta sieboldiama* leaves

showed a very strong peak in the C-H rocking (νCH_2) region at ~720 cm^{-1}, an area that also influences PC2 and further accounts for its marked positioning in PC2 away from other leaves.

While differences in various methylene frequencies were largely demonstrated by PC2, the broad hydrogen bonded OH stretching band centred at 3300 cm^{-1} was a main contributor to PC1 (Figure 6, top). As such, the positioning of the species along the horizontal axes of all the score plots in Figure 5, representing PC1, was demonstrative of the strength of this peak. As aforementioned, this peak was very weak for *Prunus laurocerasus* which explains its leftmost position in the PCA score plots. Furthermore, this peak was also weak for the *Ilex aquifolium* and *Hosta sieboldiama*, and thus they were also positioned on the left side in PC1. In contrast, the *Nymphaea odorata* had the most prominent OH stretching band, accounting for its rightmost positioning in PC1. The H-O bending modes at ca. 1630 cm^{-1} also contributed to PC1, with lower intensity peaks differentiating *Prunus laurocerasus* and *Ilex aquifolium* from the other samples. It can be surmised that PC1 was mostly influenced by ATR-FTIR peaks attributable to O-H bands (stretching ~3300 and 1630 cm^{-1}), while PC2 was most influenced by C-H methylene-related bands.

In addition to the PCA, further statistical analysis was performed using PLSR to model the leaves WCA, and hence their surface wettability from the ATR-FTIR measurements. To the Authors knowledge, this was the first time that such a model has been implemented on a complex biological system, whereby an attempt using such a system was used to determine if it was possible to relate surface chemistry and WCA. It was found that the PLSR model was able to account for ~95% of the variation in WCA with eight components. This showed that extremely variable data was able to be explained by the developed model, indicating a high level of applicability of such a system to analyse complex data. Analysing the loading plot (Figure S1) for the first three principal components for the model (PC1, 85%, black solid line; PC2, 8%, red dashed line and PC3, 5%, green dotted line), observations could be made about

the influence of various bands in the ATR-FTIR spectra that were most influential to this model, in relation to the WCA of the leaf surface. As seen following PCA, PC1 for this model was strongly influenced by the prominent OH stretching band centred at 3300 cm^{-1}, whilst PC2 was largely influenced by this peak but also the asymmetric and symmetric methylene CH_2 C-H stretching peaks at ~2916 cm^{-1} and ~2846 cm^{-1}, respectively. These bands within the loading plots were the main contributors to these principal components which attests to their importance and influence on the WCAs. Validation of the resulting regression model from this analysis indicated very good correlation ($R^2 = 0.86$) between measured and predicted values, indicating its potential for predicting surface hydrophobicity from ATR-FTIR spectra of a given surface (see Figure S2 for the plot depicting the performance of the PLSR model).

The PCA identified the *Prunus laurocerasus* and *Ilex aquifolium* surfaces as being chemically different to the other leaves. Both these surfaces demonstrated disordered (liquid-like) arrangements of long alkyl chains which may have contributed to their differentiation in the PCA. The least hydrophobic surfaces, the *Ilex aquifolium*, *Hosta sieboldiama*, and *Citrus sinensis*, had the lowest ΔG_{iwi} values of -6.0, -5.7, and -2.3 mJ/m^2, respectively. These surfaces also had the highest γ_s, γ_s^{AB}, and γ_s^- values. Differentiation in the surface topographies of the three least hydrophobic leaves was more complex compared with the more hydrophobic surfaces. However, the S_a and S_q values of the surfaces were generally lower than the other plant surfaces with the exception of the *Nymphaea odorata* and *Prunus laurocerasus*. Both the *Ilex aquifolium* and *Citrus sinensis* had surfaces with subtle features. Waxes may influence the chemical difference in the leaves and may be detected using FTIR, even if they occur as filling material within the basic cutin network (intracuticular) rather than being present on top of the cuticle (epicuticular).[35]

The *Hosta sieboldiama* was an anomaly among the leaf samples as it exhibited distinct surface features characterised by platelet-like protrusions, but was the second most wettable

surface. It also had a high γ_s^- value, in addition to a higher energy shoulder on the ν_{as} CH_2 band and a strong sharp absorption at 1640 cm^{-1} that was not present in any of the other spectra. This peak can be attributed to C=O carbonyl groups present, which demonstrated polar attributes. These features were further highlighted in the PCA, particularly with regard to the positioning within PC2. The ATR-FTIR spectrum of the *Hosta sieboldiama* exhibited a shoulder on the methylene C-H stretch at ~2925 cm^{-1}, which indicated that different hydrocarbons were present in this species. This was represented in the PCA through the distinct positioning away from the other species. These hydrocarbons may be associated with polar areas that could contribute to the high γ_s^- values. Furthermore, in the H-OH bend band, the *Hosta sieboldiama* had another absorption (1640 cm^{-1}) superimposed within the spectra, which was also accompanied by a small doublet peak at 787 and 777 cm^{-1}. These peaks may be assignable to amine or amide moieties which contributed to the high γ_s^- values recorded. These observations are likely to be related to the presence of polar domains on the *Hosta sieboldiama* leaf, which in this case, had a dominant effect on surface hydrophobicity rather than the surface topography.

The leaf surfaces studied in this work exhibited a range of different properties and yet all were water repellent and self-cleaning. An elegant explanation was offered by Zhang et al.[36] as to why droplets on surfaces with features that are associated with the highly adhesive Wenzel state can also be self-cleaning, like those surfaces that display the typical Lotus attributes associated with the Cassie-Baxter state. It is known that on surfaces consistent with Cassie-Baxter properties, self-cleaning is achieved due to low contact angle hysteresis and small hydrodynamic resistance. Zhang et al.[36] further suggested that on surfaces in the Wenzel state, small neighbouring droplets can coalesce into bigger ones, and the corresponding release of surface energy results in a transition to the Cassie-Baxter state, and therefore self-cleaning action is achieved.

Two methods of additional statistical analysis, PCA and PLSR, were used to explore and enhance the relationship between the surface chemistry characteristics, as measured using ATR-FTIR, and the surface wettability. PCA is an excellent and powerful tool to detect any underlying clusters and groupings in the data when analysing the entire surface chemistry profile. Additionally, as this technique does not make any assumptions about the data, nor does it take into account existing classifications, any notable patterns and trends found using this unsupervised approach can be confidently surmised to exist based on the ATR-FTIR spectra, not their classification. Differences seen between sample classes (i.e. hydrophobic vs less hydrophobic surfaces and different species) and the contributing factors to those differences provide insight into what distinguishes them. In our analysis, we were not only able to identify characteristics of hydrophobic leave surfaces and what are common features amongst leaves of this type, but were also able to identify species that were particularly unique and what about them was so discernible (i.e. *Prunus laurocerasus* and *Ilex aquifolium*). This analysis was based exclusively on the surface chemistry derived from ATR-FTIR spectra and clearly demonstrates the influence of surface chemistry on the wettability of leaf surfaces; the hydrophobicity of leaf surfaces is therefore not only dependent on surface topography and physicochemical properties.

Similar to PCA, the PLSR model was used to analyse the entire ATR-FTIR spectra, although this model was concerned with equating the quantitative variable, WCA, as a critical measure of surface wettability. The PLSR model found similar bands in the ATR-FTIR to be the most important at influencing surface wettability. Furthermore, the presented PLSR model showed excellent performance in validation (using a leave-one-out technique) and based on these results, it could be suggested that leaf WCA (i.e. hydrophobicity) can be predicted using ATR-FTIR surface chemistry data. As such, this finding has the potential to change the way in which surface chemistry is viewed in the design of new materials based on plant-related natural

surfaces. This is the first time such an analysis has shown the importance of surface chemistry in a range of leaf types and our produced model can be utilised to investigate and predict the water contact angle of a range of biological surfaces.

CONCLUSIONS

The physicochemical, chemical, and topographical properties of leaves obtained from twelve diverse plant varieties were examined and the results demonstrated that the most hydrophobic surfaces had low carbonyl species, ordered platelet-like structures, high roughness values, high γ_s and γ_s^{LW} values, and low γ_s^{AB} and γ_s^- values. However, regardless of the surface properties, all the leaves were self-cleaning. Using PCA, when categorising the samples according to their chemical classification, it was observed that the more hydrophobic leaves shared common surface chemistry traits, demonstrated by being grouped in close proximity with low intra-class variability. In contrast, the less hydrophobic leaves had highly-variable surface chemistry as measured by ATR-FTIR. Nevertheless, this variability in surface chemistry was able to accurately model, through PLSR, leaf water contact angle with excellent ability. This is the first time that the importance of surface chemistry in a range of leaf types has been demonstrated. As such, these results may change the way that surface chemistry is viewed in the design of new biomimetic materials based on plant surfaces. Furthermore, the presented model could be used for the fast screening and determination of the water contact angles of a range of biological surfaces.

Extensive work has been carried out on fabricating surfaces with well-defined topographical features to produce hydrophobic and self-cleaning properties. However, examples taken from nature clearly demonstrate that less hydrophobic, almost featureless surfaces may also possess self-cleaning and non-wetting properties. A complete understanding of the interactions between the magnitude and shape of surface topography, chemistry, and

physiochemistry, in addition to their influence on the self-cleaning action of surfaces has still not been elucidated. In future work, we intend to design novel surfaces based on these parameters and assess their self-cleaning properties in a range of experimental assays to determine their use in specific, applied applications.

FUNDING

This work was supported by the European Union's Horizon 2020 research and innovation programme under grant agreement No 952471

ASSOCIATED CONTENT

The Supporting Information is available free of charge at

Table providing surface free energy components of test liquids; Graphs predicting the WCAs from the ATR-FTIR using PLSR.

CONFLICTS OF INTEREST

The authors declare no competing financial interest.

REFERENCES

(1) Hsu, S.-H.; Woan, K.; Sigmund, W. Biologically Inspired Hairy Structures for Superhydrophobicity. *Mater. Sci. Eng. R Reports* **2011**, *72*, 189–201. https://doi.org/10.1016/j.mser.2011.05.001.

(2) Wang, G.; Guo, Z.; Liu, W. Interfacial Effects of Superhydrophobic Plant Surfaces: A Review. *J. Bionic Eng.* **2014**, *11*, 325–345. https://doi.org/10.1016/S1672-6529(14)60047-0.

(3) Barthlott, W.; Mail, M.; Neinhuis, C. Superhydrophobic Hierarchically Structured Surfaces in Biology: Evolution, Structural Principles and Biomimetic Applications. *Philos. Trans. R. Soc. A Math. Phys. Eng. Sci.* **2016**, *374*, 20160191. https://doi.org/10.1098/rsta.2016.0191.

(4) Barthlott, W.; Neinhuis, C. Purity of the Sacred Lotus, or Escape from Contamination in Biological Surfaces. *Planta* **1997**, *202*, 1–8. https://doi.org/10.1007/s004250050096.

(5) Peter, A.; Lutey, A. H. A.; Faas, S.; Romoli, L.; Onuseit, V.; Graf, T. Direct Laser Interference Patterning of Stainless Steel by Ultrashort Pulses for Antibacterial Surfaces. *Opt. Laser Technol.* **2020**, *123*, 105954. https://doi.org/10.1016/j.optlastec.2019.105954.

(6) Rajab, F. H.; Liauw, C. M.; Benson, P. S.; Li, L.; Whitehead, K. A. Production of Hybrid Macro/Micro/Nano Surface Structures on Ti6Al4V Surfaces by Picosecond Laser Surface Texturing and Their Antifouling Characteristics. *Colloids Surfaces B Biointerfaces* **2017**, *160*, 688–696. https://doi.org/10.1016/j.colsurfb.2017.10.008.

(7) Rajab, F. H.; Liauw, C. M.; Benson, P. S.; Li, L.; Whitehead, K. A. Picosecond Laser Treatment Production of Hierarchical Structured Stainless Steel to Reduce Bacterial Fouling. *Food Bioprod. Process.* **2018**, *109*, 29–40. https://doi.org/10.1016/j.fbp.2018.02.009.

(8) Lutey, A. H. A.; Gemini, L.; Romoli, L.; Lazzini, G.; Fuso, F.; Faucon, M.; Kling, R. Towards Laser-Textured Antibacterial Surfaces. *Sci. Rep.* **2018**, *8*, 10112. https://doi.org/10.1038/s41598-018-28454-2.

(9) Aryal, B.; Neuner, G. Leaf Wettability Decreases along an Extreme Altitudinal Gradient. *Oecologia* **2010**, *162*, 1–9. https://doi.org/10.1007/s00442-009-1437-3.

(10) Ensikat, H. J.; Ditsche-Kuru, P.; Neinhuis, C.; Barthlott, W. Superhydrophobicity in Perfection: The Outstanding Properties of the Lotus Leaf. *Beilstein J. Nanotechnol.* **2011**, *2*, 152–161. https://doi.org/10.3762/bjnano.2.19.

(11) Balsdon, J. A.; Braman, S. K.; Espelie, K. E. Biology and Ecology of Anagrus Takeyanus (Hymenoptera: Mymaridae), an Egg Parasitoid of the Azalea Lace Bug (Heteroptera: Tingidae). *Environ. Entomol.* **1996**, *25*, 383–389. https://doi.org/10.1093/ee/25.2.383.

(12) Wang, Y.; Braman, S. K.; Robacker, C. D.; Latimer, J. G.; Espelie, K. E. Composition and Variability of Epicuticular Lipids of Azaleas and Their Relationship to Azalea Lace Bug Resistance. *J. Am. Soc. Hortic. Sci.* **1999**, *124*, 239–244. https://doi.org/10.21273/jashs.124.3.239.

(13) Jetter, R.; Schäffer, S.; Riederer, M. Leaf Cuticular Waxes Are Arranged in Chemically and Mechanically Distinct Layers: Evidence from Prunus Laurocerasus L. *Plant, Cell Environ.* **2000**, *23*, 619–628. https://doi.org/10.1046/j.1365-3040.2000.00581.x.

(14) Ribeiro da Luz, B. Attenuated Total Reflectance Spectroscopy of Plant Leaves: A Tool for Ecological and Botanical Studies. *New Phytol.* **2006**, *172*, 305–318. https://doi.org/10.1111/j.1469-8137.2006.01823.x.

(15) J. A. Hardin; C. L. Jones; P. R. Weckler; N. O. Maness; Madden, R. D. Rapid Quantification of Spinach Leaf Cuticular Wax Using Fourier Transform Infrared Attenuated Total Reflectance Spectroscopy. *Trans. ASABE* **2013**, *56*, 331–339. https://doi.org/10.13031/2013.42579.

(16) Tu, C.-W.; Tsai, C.-H.; Wang, C.-F.; Kuo, S.-W.; Chang, F.-C. Fabrication of Superhydrophobic and Superoleophilic Polystyrene Surfaces by a Facile One-Step

554 Method. *Macromol. Rapid Commun.* **2007**, *28*, 2262–2266.
555 https://doi.org/10.1002/marc.200700447.

556 (17) Wang, H.; Shi, H.; Li, Y.; Wang, Y. The Effects of Leaf Roughness, Surface Free
557 Energy and Work of Adhesion on Leaf Water Drop Adhesion. *PLoS One* **2014**, *9*,
558 e107062. https://doi.org/10.1371/journal.pone.0107062.

559 (18) van Oss, C. J.; Good, R. J.; Chaudhury, M. K. The Role of van Der Waals Forces and
560 Hydrogen Bonds in "Hydrophobic Interactions" between Biopolymers and Low
561 Energy Surfaces. *J. Colloid Interface Sci.* **1986**, *111*, 378–390.
562 https://doi.org/10.1016/0021-9797(86)90041-X.

563 (19) van Oss, C. J. Hydrophobicity of Biosurfaces - Origin, Quantitative Determination and
564 Interaction Energies. *Colloids Surfaces B Biointerfaces* **1995**, *5*, 91–110.
565 https://doi.org/10.1016/0927-7765(95)01217-7.

566 (20) van Oss, C. J.; Giese, R. F. The Hydrophilicity and Hydrophobicity of Clay Minerals.
567 *Clays Clay Miner.* **1995**, *43*, 474–477. https://doi.org/10.1346/CCMN.1995.0430411.

568 (21) Bos, R.; Busscher, H. J. Role of Acid-Base Interactions on the Adhesion of Oral
569 Streptococci and Actinomyces to Hexadecane and Chloroform - Influence of Divalent
570 Cations and Comparison between Free Energies of Partitioning and Free Energies
571 Obtained by Extended DLVO Analysis. *Colloids Surfaces B Biointerfaces* **1999**, *14*,
572 169–177. https://doi.org/10.1016/S0927-7765(99)00034-X.

573 (22) Skovager, A.; Whitehead, K.; Wickens, D.; Verran, J.; Ingmer, H.; Arneborg, N. A
574 Comparative Study of Fine Polished Stainless Steel, TiN and TiN/Ag Surfaces:
575 Adhesion and Attachment Strength of Listeria Monocytogenes as Well as Anti-
576 Listerial Effect. *Colloids Surfaces B Biointerfaces* **2013**, *109*, 190–196.
577 https://doi.org/10.1016/j.colsurfb.2013.03.044.

(23) Whitehead, K. A.; Smith, L. A.; Verran, J. The Detection and Influence of Food Soils on Microorganisms on Stainless Steel Using Scanning Electron Microscopy and Epifluorescence Microscopy. *Int. J. Food Microbiol.* **2010**, *141*, S125–S133. https://doi.org/10.1016/j.ijfoodmicro.2010.01.012.

(24) Mirabella, F. M. *Principles, Theory, and Practice of Internal Reflection Spectroscopy*; 2006. https://doi.org/10.1201/9781003066941-2.

(25) Team, R. C. The R Project For Statistical Computing. 2015.

(26) Team, R. C. A Language And Environment For Statistical Computing. 2015.

(27) Wickham, H. Elegant Graphics For Data Analysis. 2016.

(28) Mevik, B.-H.; Wehrens, R.; Liland, K. H. Suggests, Package 'Pls.' 2019.

(29) Camacho, J.; Picó, J.; Ferrer, A. Data Understanding with PCA: Structural and Variance Information Plots. *Chemom. Intell. Lab. Syst.* **2010**, *100*, 48–56. https://doi.org/10.1016/j.chemolab.2009.10.005.

(30) Schulte, A. J.; Droste, D. M.; Koch, K.; Barthlott, W. Hierarchically Structured Superhydrophobic Flowers with Low Hysteresis of the Wild Pansy (Viola Tricolor) - New Design Principles for Biomimetic Materials. *Beilstein J. Nanotechnol.* **2011**, *2*, 228–236. https://doi.org/10.3762/bjnano.2.27.

(31) Nosonovsky, M.; Bhushan, B. Biomimetic Superhydrophobic Surfaces: Multiscale Approach. *Nano Lett.* **2007**, *7*, 2633–2637. https://doi.org/10.1021/nl071023f.

(32) Bhushan, B.; Jung, Y. C. Micro- and Nanoscale Characterization of Hydrophobic and Hydrophilic Leaf Surfaces. *Nanotechnology* **2006**, *17*, 2758–2772. https://doi.org/10.1088/0957-4484/17/11/008.

(33) Godeau, G.; Laugier, J.-P.; Orange, F.; Godeau, R.-P.; Guittard, F.; Darmanin, T. A Travel in the Echeveria Genus Wettability's World. *Appl. Surf. Sci.* **2017**, *411*, 291–302. https://doi.org/10.1016/j.apsusc.2017.03.192.

(34) BOYCE, R. L.; McCUNE, D. C.; BERLYN, G. P. A Comparison of Foliar Wettability of Red Spruce and Balsam Fir Growing at High Elevation. *New Phytol.* **1991**, *117*, 543–555. https://doi.org/10.1111/j.1469-8137.1991.tb00959.x.

(35) Barthlott, W.; Mail, M.; Bhushan, B.; Koch, K. Plant Surfaces: Structures and Functions for Biomimetic Innovations. *Nano-Micro Lett.* **2017**, *9*, 23. https://doi.org/10.1007/s40820-016-0125-1.

(36) Zhang, K.; Li, Z.; Maxey, M.; Chen, S.; Karniadakis, G. E. Self-Cleaning of Hydrophobic Rough Surfaces by Coalescence-Induced Wetting Transition. *Langmuir* **2019**, *35*, 2431–2442. https://doi.org/10.1021/acs.langmuir.8b03664.

614 TOC Graphic

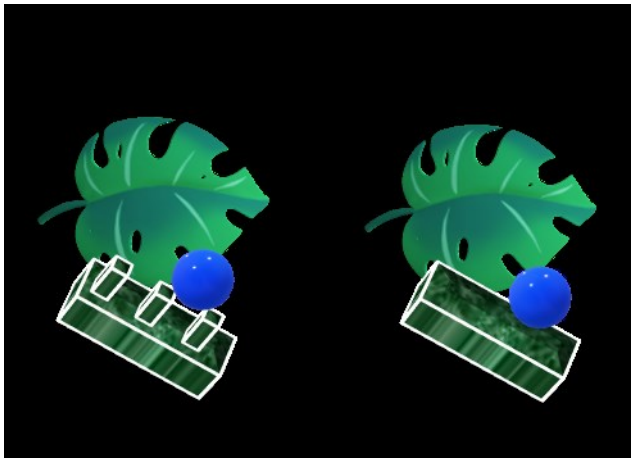

615